Rod-Coil Type Miktoarm Star Copolymers Consisting of Polyfluorene and Polylactide: Precise Synthesis and Structure-Morphology Relationship‡

Kengo Saito,[†] Takuya Isono,[†] Han-Sheng Sun,[¶] Toyoji Kakuchi,[†] Wen-Chang Chen,[¶,*] Toshifumi Satoh[†,*]

[†]Graduate School of Chemical Sciences and Engineering and Division of Applied Chemistry, Faculty of Engineering, Hokkaido University, Sapporo 060-8628, Japan

[¶]Department of Chemical Engineering, National Taiwan University, Taipei 10617, Taiwan

[*]To whom correspondence should be addressed: Wen-Chang Chen (chenwc@ntu.edu.tw) & Toshifumi Satoh (satoh@poly-bm.eng.hokudai.ac.jp)

‡Electronic supplementary information (ESI) available: Additional figures.

Abstract. A series of rod-coil miktoarm star copolymers consisting of poly[2,7-(9,9-dihexylfluorene)] (PF) and polylactide (PLA) arms as the rod and coil segments, respectively, were synthesized by combining the chain-growth Suzuki-Miyaura coupling polymerization and living ring-opening polymerization (ROP). First, PFs having a hydroxyl group at the α-chain end (PF-BnOH) were prepared by the polymerization of 2-(7-bromo-9,9-dihexyl-9*H*-fluorene-2-yl)4,4,5,5-tetramethyl-1,2,3-dioxaborolane using the initiating system of 4-(tetrahydropyran-2'-yloxymethyl)-iodobenzene/$Pd_2(dba)_3$/*t*-Bu_3P. After a couple of chain end modifications, PFs having one, two, and three hydroxyl groups at the α-chain end (PF-OH, PF-$(OH)_2$, and PF-$(OH)_3$, respectively) were obtained with the dispersity (*Đ*) values of less than 1.29. The obtained PF-OH, PF-$(OH)_2$, and PF-$(OH)_3$ were used as the initiator for the organic base-catalyzed ROP of *rac*-lactide to produce the AB type linear diblock (PF-*b*-PLA) and AB_2 and AB_3 type miktoarm star copolymers (PF-*b*-$(PLA)_2$ and PF-*b*-$(PLA)_3$, respectively). The self-assembled nanostructures in the thermally-annealed PF-*b*-$(PLA)_x$s (x = 1, 2, and 3) were evaluated in the bulk by synchrotron small angle X-ray scattering (SAXS) and transmission electron microscopy (TEM). The PF-*b*-PLA, PF-*b*-$(PLA)_2$, and PF-*b*-$(PLA)_3$ with the PF weight fractions of 0.52 – 0.56 were found to form poorly ordered PLA cylindrical structures in the PF matrix due to the strong rod-rod interaction of the PF segment. On the other hand, these BCPs with the PF weight fractions of 0.22 – 0.23 exhibited the hexagonally close-packed cylinder (Hex) morphologies, in which the cylindrical PF phase was embedded in the PLA matrix. More interestingly, the

domain-spacing (*d*) values for the Hex morphologies decreased with the increasing PLA arm number despite each BCP having a comparable molecular weight and PF weight fraction: d = 26.4 nm for PF-*b*-PLA, d = 21.7 nm for PF-*b*-$(PLA)_2$, and d = 18.6 nm for PF-*b*-$(PLA)_3$.

Introduction

Recent progress in synthetic polymer chemistry has enabled us to design and synthesize a wide array of macromolecules with complex architectures, such as star, comb, cyclic, and multicyclic shapes, which provided further insight into their structure-property relationship and expanded the scope of the potential applications of polymeric materials.[1-5] Among the architecturally-complex macromolecules, the miktoarm star copolymer,[6,7] which is one of the star-shaped copolymers that is composed of more than two chemically distinct polymer arms, is of particular interest because of its block copolymer (BCP)-like nature to form miceller aggregates in solution and microphase-separated structures in the bulk, whose nano-ordered structures can be varied by modulating the arm number and arm length.[8]

For the coil-coil BCP system, a significant effort have been devoted to understanding the relationship between the macromolecular architectures and resulting self-assembled structures by employing precisely synthesized BCP samples. For example, Hadjichristidis and coworkers intensively studied the preparation of coil-coil miktoarm star copolymers consisting of polystyrene and polyisoprene arms via the living anionic polymerization combined with chlorosilane compounds.[6,9-12] Meanwhile, Hirao and coworkers established an iterative route based on the living anionic polymerization to a wide array of miktoarm star copolymers containing two or more different polymer arms.[13-18] In addition, the combination of living radical polymerizations and living ring-opening polymerizations have been successfully utilized to create miktoarm star copolymers

consisting of various kinds of polymer arms.[19-22] However, a challenge still exists in the precise synthesis of miktoarm star polymers containing rod-like blocks mainly due to the difficulty in the preparation of the well-defined rod-like polymer segment. Although several pioneering studies concerning the miktoarm star polymers containing rod-like blocks, such as poly(L-glutamic acid),[23,24] poly(*n*-hexyl isocyanate),[25-28] and poly(3-alkylthiopehe)s,[29-31] have been reported, the effect of the miktoarm type architectures on the self-assembling behaviors remains largely unexplored.

The main-chain conjugated polymer, such as poly(phenylene)s, poly(phenylenevinylene)s, poly(thiophene)s, and poly(fluorene)s, is the most important class of rod-like polymers, whose distinctive opto-electronic properties are highly interesting for creating organic devices, such as sensors,[32,33] organic light-emitting diodes (OLED),[34-36] organic field-effect transistors (OFET),[37,38] organic photovoltaics (OPV),[39-41] and memory devices.[42,43] Among them, poly(fluorene)s are highly promising materials for such applications because of their high fluorescence quantum yield and excellent charge carrier mobility.[44,45] However, the strong π-π stacking interaction between the PF chains leads to forming randomly oriented aggregates, resulting in the significant loss of the device performance.[46,47] On the other hand, it had been found that the BCPs consisting of PF and coil blocks self-assembled into certain nanostructures with a controlled PF chain orientation,[48-51] which might be beneficial for improving the PF-based device performance. For example, we discovered that the triblock copolymers of

poly[2,7-(9,9-dihexylfluorene)]-*b*-poly(*N*-isopropylacrylamide)-*b*-poly(*N*-methylolacrylamide)s and their electrospun nanofibers could form ordered lamellar structures to optimize their photophysical properties for sensing applications.[52] Therefore, the control of the self-assembled nanostructures of the PF-based rod-coil BCPs through the design of a macromolecular architecture should be of fundamental interest.

In order to study the correlation between the macromolecular architecture and self-assembled nanostructures in PF-based rod-coil BCPs, we now report the synthesis of a series of PF-based rod-coil BCPs consisting of poly[2,7-(9,9-dihexylfluorene)] (PF, as A block) and polylactide (PLA, as B block) with AB_2 and AB_3 type miktoarm star-shaped architectures by controlled/living polymerization methods. The corresponding linear AB type BCPs were also prepared for comparison. We employed PLA as the coil block, which is highly desirable for future applications because the PLA can be easily removed from the self-assembled nanostructures by hydrolysis, leading to nanopatterned arrays of the PF chain.[53] Our synthetic strategy for the linear diblock and miktoarm star copolymers is outlined in Scheme 1. First, the PF macroinitiators possessing hydroxyl groups at the α-chain end were prepared via the chain growth Suzuki-Miyaura coupling polymerization[54,55] and subsequent chain end modifications in which the hydroxyl groups on the macroinitiators served as the initiating sites for the subsequent ROP. The obtained macroinitiators were then subjected to the living ROP of *rac*-lactide (*rac*-LA), leading to the AB_2 and AB_3 type miktoarm star copolymers, i.e., PF-*b*-$(PLA)_2$ and PF-*b*-$(PLA)_3$, respectively, as well as

the corresponding AB type linear diblock copolymers, i.e., PF-*b*-PLA. The preliminary study of the self-assembled nanostructure of the obtained BCPs was performed on the bulk samples by small angle X-ray scattering and transmission electron microscopy.

Scheme 1. Synthetic pathways for linear diblock (PF-*b*-PLA) and miktoarm star copolymers (PF-*b*-$(PLA)_2$ and PF-*b*-$(PLA)_3$) consisting of poly[2,7-(9,9-dihexylfluorene)] (PF) and polylactide (PLA)

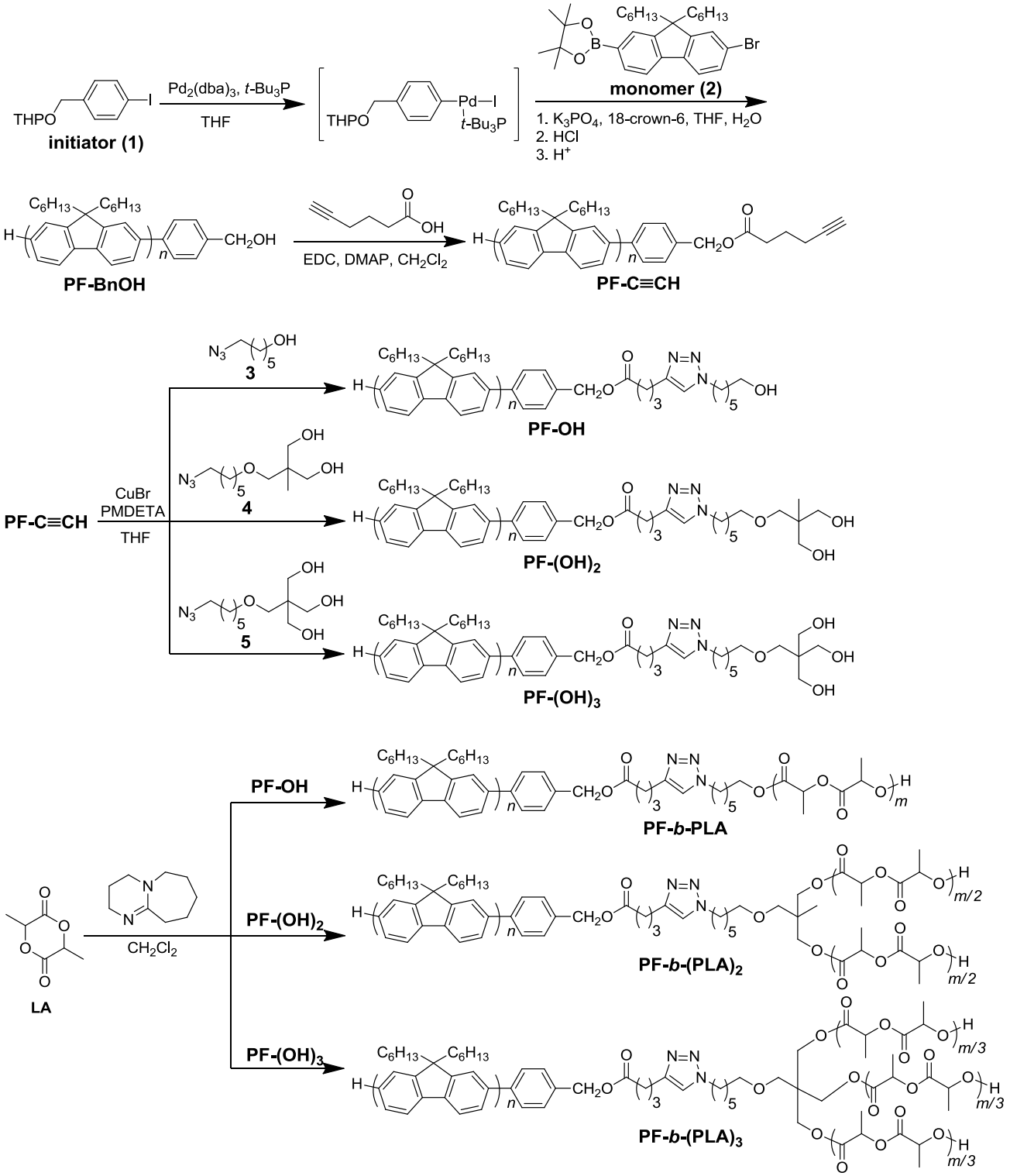

Experimental

Materials. 4-(Tetrahydropyran-2'-yloxymethyl)-iodobenzene (**1**),[56] 2-(7-bromo-9,9-dihexyl-9*H*-fluorene-2-yl)4,4,5,5-tetramethyl-1,2,3-dioxaborolane (**2**),[57,58] 6-azido-1-hexanol (**3**),[59] 2-[(6-azidohexyloxy)methyl]-2-methylpropane-1,3-diol (**4**),[60] and 2-[(6-azidohexyloxy)methyl]-2-(hydroxylmethyl)propane-1,3-diol (**5**)[60] were prepared according to reported methods. 1-Ethyl-3-(3-dimethylaminopropyl)carbodiimide hydrochloride (EDC; TCI, >98.0%), 18-crown-6 (TCI, >98%), 5-hexynoic acid (TCI, >95%), 4-dimethylaminopyridine (DMAP; TCI, >99.0%), *N*,*N*,*N*',*N*'',*N*''-pentamethyldiethylenetriamine (PMDETA; TCI, >99.0%), tris(dibenzyldeneacetone)palladium ($Pd_2(dba)_3$; Aldrich; >97.0%), CuCl (Aldrich; 99.995%), tri(*t*-butyl)phosphine (*t*-Bu_3P; Wako Pure Chemicals; >96.0%), and tripotassium phosphate (Wako Pure Chemicals; >95.0%) were purchased from commercial resources and used as received. *rac*-Lactide (*rac*-LA; TCI; >98%) was purified by recrystallization (twice) from dry toluene and stored in a glovebox. 1,8-Diazabicyclo[5.4.0]undec-7-ene (DBU; TCI; >98.0%) was purified by distillation over CaH_2 under reduced pressure and stored in the glovebox. Commercially-available dry CH_2Cl_2 (Kanto Chemical Co., Inc., >99.5%, water content, <0.001%) was further purified by an MBRAUN MB SPS Compact solvent purification system equipped with a MB-KOL-C column and a MB-KOL-A column, which was then directly used for the polymerizations. Commercially-available dry THF (Kanto Chemical Co., Inc., >99.5%, water content, <0.001%) was further purified by an MBRAUN MB SPS Compact solvent purification system equipped with a

MB-KOL-C column and a MB-KOL-A column, which was then directly used for the polymerizations.

Instruments. The polymerization was carried out in an MBRAUN stainless steel glovebox equipped with a gas purification system (molecular sieves and copper catalyst) in a dry argon atmosphere (H_2O, O_2 <1 ppm). The moisture and oxygen contents in the glovebox were monitored by an MB-MO-SE 1 moisture sensor and an MB-OX-SE 1 oxygen sensor, respectively. The ^{1}H (400 MHz) and ^{13}C NMR (100 MHz) spectra were obtained using a JEOL JNM-ESC400 instrument at room temperature. The size exclusion chromatography (SEC) was performed at 40 °C using a Jasco high-performance liquid chromatography system (PU-2080Plus Intelligent HPLC pump, CO-2065Plus Column oven, RI-2031Plus Intelligent RI detector, and Shodex DG-2080-54) equipped with a Shodex KF-G guard column (4.6 mm × 10 mm; particle size, 8 μm) and two Shodex KF-804 columns (linear; particle size, 7 μm; 8.0 mm × 300 mm; exclusion limit, 4×10^5) in THF at the flow rate of 1.0 mL min^{-1}. The number-average molecular weight ($M_{n,SEC}$) and dispersity ($Đ$) of the polymer were calculated on the basis of a polystyrene calibration. Matrix-assisted laser desorption ionization time-of-flight mass spectrometry (MALDI-TOF MS) measurement of the obtained polymer was carried out in the reflector mode using an Applied Biosystems Voyager-DE STR-H equipped with a 337-nm nitrogen laser (3-ns pulse width). The sample for the MALDI-TOF MS measurement was prepared by drop-casting the mixture of a polymer solution (5 μL; 1 g L^{-1} in THF) and saturated

trans-2-[3-(4-*tert*-butylphenyl)-2-methyl-2-propylidene]malononitrile solution (200 μL; in THF) on a sample plate. The thermogravimetric analysis (TGA) was performed under a nitrogen atmosphere up to 800 °C at the heating rate of 10 °C min^{-1} using a TA Instruments TGA Q50. The differential scanning calorimetry (DSC) was performed under a nitrogen atmosphere at 30 to 200 °C at the heating rate of 5 °C min^{-1} and the cooling rate of -5 °C min^{-1} using a TA Instruments DSC Q100.

Synthesis of poly[2,7-(9,9-dihexylfluorene)] (PF-BnOH) having a benzyl alcohol moiety at the *α*-chain end. The PF-BnOHs were prepared according to reported method with further modifications.[57,58] A typical procedure for the synthesis of PF-BnOH is as follows (Procedure A): In the glovebox, **1** (1.14 mL, 0.72 mmo, as 0.63 mol L^{-1} stock solution in THF), $Pd_2(dba)_3$ (396 mg, 1.7 mmol), and *t*-Bu_3P (3.46 mL, 1.7 mmol, as 0.5 mol L^{-1} stock solution in THF) were placed in a vial containing THF (15 mL) and dissolved. After stirring for 1 h at room temperature, the mixture was passed through a 0.45 mm PTFE filter to produce Pd-initiator solution. The vial containing the stock solution of the Pd-initiator was sealed and taken out of the glovebox. In a 1000-mL three-necked round bottom flask, K_3PO_4 (22.9 g, 108 mmol) and 18-crown-6 (9.51 g, 36.0 mmol) were dissolved in a mixed solvent of THF (420 mL) and deionized water (54 mL) that had been deoxygenated by argon bubbling at least for 1 h. The stock solution of the Pd-initiator was transferred to the flask using a cannula under an argon atmosphere, and the entire mixture was cooled to -10 °C. **2** (8.50 mL, 3.57 mmol, as 0.42 mol L^{-1} stock solution in THF) was quickly added to the mixture under an argon atmosphere, and the entire mixture was vigorously stirred for

1.5 h at -10 °C. To the reaction mixture, 12 mol L^{-1} HCl (50 mL) was added to terminate the polymerization. The solvent was removed by evaporation, and the residue was dissolved in CH_2Cl_2 and washed with brine. The organic layer was dried over $MgSO_4$ and concentrated. The resulting residue was purified by passing it through a pad of alumina and eluted with THF. The eluent was treated with Dowex 50W-X2-200 for 20 h at room temperature to remove the THP protecting group. After filtration, the resulting solution was concentrated and precipitated using THF as a good solvent and cold MeOH as a poor solvent to give PF_{5k}-BnOH (1.10 g) as a light yellow powder. Yield: 91.4%. $M_{n,SEC}$ = 6300 g mol^{-1}; $M_{n,NMR}$ = 4800 g mol^{-1}, $Đ$ = 1.34. ^{1}H NMR (400 MHz, $CDCl_3$): δ (ppm) 7.93-7.77 (m, Ar-*H*), 7.75-7.57 (m, Ar-*H*), 7.50 (d, Ar-*H*), 4.79 (d, -C*H*$_2$OH), 2.12 (br, -C*H*$_2$(CH$_2$)$_4$CH$_3$), 1.36-0.66 (m, -CH$_2$(C*H*$_2$)$_4$C*H*$_3$).

Synthesis of poly[2,7-(9,9-dihexylfluorene)] (PF-C≡CH) having an ethynyl moiety at the α-chain end. In a 200-mL three-necked flask, PF_{5k}-BnOH ($M_{n,NMR}$ = 4800 g mol^{-1}; 965 mg, 0.10 mmol), EDC (196 mg, 1.0 mmol), and DMAP (125 mg, 1.0 mmol) were vacuum dried for 9 h. A solution of 5-hexynoic acid (113 μL, 1.0 mmol) in dry CH_2Cl_2 (100 mL) that had been deoxygenated by Ar bubbling was transferred to the flask via a cannula under an argon atmosphere. After stirring for 24 h at room temperature, the solvent was evaporated to dryness. The residue was purified by reprecipitation using THF as a good solvent and cold MeOH as a poor solvent to give PF-C≡CH (950 mg) as a light yellow powder. Yield: 98.4%. $M_{n,SEC}$ = 7300 g mol^{-1}, $M_{n,NMR}$ = 4900 g mol^{-1}, $Đ$ = 1.31. ^{1}H NMR (400 MHz, $CDCl_3$): δ (ppm) 7.92-7.77 (m, Ar-*H*), 7.73-7.55 (m,

Ar-*H*), 7.48 (d, Ar-*H*), 5.20 (s, -CH_2-OC(=O)CH_2-), 2.55 (t, -OC(=O)CH_2-), 2.30 (m, CH_2C≡CH), 2.12 (br, -CH_2(CH_2)$_4$$CH_3$), 1.98 (t, -C≡C*H*), 1.91 (m, -C$H_2$$CH_2$C≡CH), 1.39-0.58 (m, -$CH_2$(C$H_2$)$_4CH_3$).

Synthesis of PF-OH Macroinitiator. A typical procedure for the macroinitiator synthesis is as follows (Procedure B): In a Schlenk flask, PF_{5k}-C≡CH ($M_{n,NMR}$ = 4900 g mol^{-1}; 300 mg, 31.3 μmol) and CuCl (9.3 mg, 94 μmol) were vacuum dried for 9 h. A solution of PMDETA (40.0 μL, 188 μmol) and **3** (22.4 mg, 156 μmol) in THF (5.0 mL) that had been deoxygenated by Ar bubbling was transferred to the Schlenk flask via a cannula under an argon atmosphere. After stirring for 48 h at room temperature, the mixture was passed through a pad of alumina and eluted with THF to remove the copper catalyst. The eluate was subjected to evaporation and the resulting residue was purified by reprecipitation using THF as a good solvent and cold MeOH as a poor solvent to give PF_{5k}-OH macroinitiator (285 mg) as a light yellow powder. Yield: 95.0%. $M_{n,SEC}$ = 7800 g mol^{-1}, $M_{n,NMR}$ = 5000 g mol^{-1}, $Đ$ = 1.29. ^{1}H NMR (400 MHz, $CDCl_3$): δ (ppm) 7.92-7.78 (m, Ar-*H*), 7.75-7.56 (m, Ar-*H*), 7.48 (d, Ar-*H*), 5.19 (s, -CH_2-OC(=O)CH_2-), 4.32 (t, -CH_2(CH_2)$_5$OH), 3.63 (m, -CH_2OH), 2.79 (t, -OC(=O)CH_2CH_2CH_2-), 2.47 (t, -OC(=O)CH_2CH_2CH_2-), 2.12 (br, -CH_2(CH_2)$_4$$CH_3$), 1.90 (m, -OC(=O)C$H_2CH_2CH_2$-), 1.46-0.62 (m, -$CH_2$(C$H_2$)$_4CH_3$).

Synthesis of PF-(OH)$_2$ Macroinitiator. Procedure B was used for the click reaction of PF_{5k}-C≡CH ($M_{n,NMR}$ = 4900 g mol^{-1}; 300 mg, 31.3 μmol) with CuCl (9.3 mg, 94 μmol), PMDETA (40 μL, 188 μmol), and **4** (38.3 mg, 156 μmol) in THF (5.0 mL) to form the PF_{5k}-$(OH)_2$

macroinitiator (237 mg) as a light yellow powder. Yield: 79.0%. $M_{n,SEC}$ = 9300 g mol^{-1}; $M_{n,NMR}$ = 5500 g mol^{-1}; $Đ$ = 1.22. ^{1}H NMR (100 MHz, $CDCl_3$): δ (ppm) 7.92-7.78 (m, Ar-*H*), 7.77-7.57 (m, Ar-*H*), 7.47 (d, Ar-*H*), 5.19 (s, -C*H*$_2$-OC(=O)CH$_2$-), 4.32 (t, -C*H*$_2$(CH$_2$)$_5$O-), 3.73-3.54 (m, C*H*$_2$OH), 3.46-3.36 (m, -C*H*$_2$OC*H*$_2$-), 2.80 (t, -OC(=O)CH$_2$CH$_2$C*H*$_2$-), 2.47 (t, -OC(=O)C*H*$_2$CH$_2$CH$_2$-), 2.12 (br, -C*H*$_2$(CH$_2$)$_4$CH$_3$), 1.90 (m, -OC(=O)CH$_2$C*H*$_2$CH$_2$-), 1.46-0.62 (m, -CH$_2$(C*H*$_2$)$_4$C*H*$_3$).

Synthesis of PF-(OH)$_3$ Macroinitiator. Procedure B was used for the click reaction of PF-C≡CH ($M_{n,NMR}$ = 4900 g mol^{-1}; 300 mg, 31.3 μmol) with CuCl (9.3 mg, 94 μmol), PMDETA (40 mL, 188 μmol), and **5** (40.8 mg, 156 μmol) in THF (5.0 mL) to form the PF$_{5k}$-(OH)$_3$ macroinitiator (144 mg) as a light yellow powder. Yield: 48.0%. $M_{n,SEC}$ = 9400 g mol^{-1}; $M_{n,NMR}$ = 5500 g mol^{-1}; $Đ$ = 1.21. ^{1}H NMR (400 MHz, $CDCl_3$): δ (ppm) 7.92-7.78 (m, Ar-*H*), 7.77-7.57 (m, Ar-*H*), 7.47 (d, Ar-*H*), 5.19 (s, -C*H*$_2$-OC(=O)CH$_2$-), 4.33 (t, -C*H*$_2$(CH$_2$)$_5$O-), 3.75 (d, C*H*$_2$OH), 3.46-3.36 (m, -C*H*$_2$OC*H*$_2$-), 2.80 (t, CH$_2$O*H*), 2.74 (t, -OC(=O)CH$_2$CH$_2$C*H*$_2$-), 2.47 (t, -OC(=O)C*H*$_2$CH$_2$CH$_2$-), 2.12 (br, -C*H*$_2$(CH$_2$)$_4$CH$_3$), 1.90 (m, -OC(=O)CH$_2$C*H*$_2$CH$_2$-), 1.46-0.62 (m, -CH$_2$(C*H*$_2$)$_4$C*H*$_3$).

Synthesis of PF-*b*-PLA. A typical procedure for the ROP of lactide using the PF macroinitiator is as follows (Procedure C): In a glovebox, DBU (1.5 μL, 15 μmol) was added to a stirred solution of the PF$_{5k}$-OH macroinitiator ($M_{n,NMR}$ = 5000 g mol^{-1}; 203 mg, 40.6 μmol) and *rac*-LA (214 mg, 1.48 mmol) in CH_2Cl_2 (1.49 mL). After 10 min, an excess of benzoic acid (ca. 2 mg) was added to the reaction mixture to terminate the polymerization. The mixture was purified by reprecipitation using THF as a good solvent and cold MeOH as a poor solvent to give PF$_{5k}$-*b*-PLA

(319 mg) as a light yellow powder. Yield: 76.5%. $M_{n,SEC}$ = 12000 g mol^{-1}; $M_{n,NMR}$ = 9400 g mol^{-1}; $Đ$ = 1.15. ^{1}H NMR ($CDCl_3$, 400MHz) ppm: 7.85-7.20 (m, Ar-*H*), 5.19 (m, -C(=O)C*H*CH_3O-), 4.40-4.25 (m, -C*H*$_2$(CH_2)$_5$O-, -C(=O)C*H*CH_3OH), 4.14 (t, -(CH_2)$_5$C*H*$_2$O-), 2.80 (t, -OC(=O)CH_2CH_2C*H*$_2$-), 2.47 (t, -OC(=O)C*H*$_2CH_2CH_2$-), 2.12 (br, -C*H*$_2$(CH_2)$_4$$CH_3$), 1.89 (m, -OC(=O)$CH_2$C*H*$_2CH_2$-), 1.58 (m, -C(=O)C*H*$_3$CHO-), 1.40-0.60 (m, -$CH_2$(C*H*$_2$)$_4$C*H*$_3$).

Synthesis of PF-*b*-(PLA)$_2$. Procedure C was used for the ROP of *rac*-LA (178 mg, 1.23 mmol) using the PF$_{5k}$-(OH)$_2$ macroinitiator ($M_{n,NMR}$ = 5500 g mol^{-1}; 168 mg, 30.5 μmol) and DBU (1.8 μL, 12 μmol) in CH_2Cl_2 (1.24 mL) for 8 min to produce PF$_{5k}$-*b*-(PLA)$_2$ (293 mg) as a light yellow powder. Yield: 84.7%. $M_{n,SEC}$ = 12200 g mol^{-1}; $M_{n,NMR}$ = 9800 g mol^{-1}; $Đ$ = 1.17. ^{1}H NMR ($CDCl_3$, 400MHz) ppm: 7.85-7.20 (m, Ar-*H*), 5.19 (m, -C(=O)C*H*CH_3O), 4.45-4.27 (m, -C*H*$_2$(CH_2)$_5$O-, -C(=O)C*H*CH_3OH), 4.14 (t, -CCH_3(C*H*$_2$O-PLA)$_2$), 3.34 (t, -C*H*$_2$(CH_2)$_5$O-), 3.21 (s, -CH_2(CH_2)$_5$OC*H*$_2$-), 2.80 (t, -OC(=O)CH_2CH_2C*H*$_2$-), 2.45 (t, -OC(=O)C*H*$_2CH_2CH_2$-), 2.12 (br, -C*H*$_2$(CH_2)$_4$$CH_3$), 1.89 (m, -OC(=O)$CH_2$C*H*$_2CH_2$-), 1.58 (m, -C(=O)C*H*$_3$CHO-), 1.40-0.60 (m, -$CH_2$(C*H*$_2$)$_4$C*H*$_3$).

Synthesis of PF-*b*-(PLA)$_3$. Procedure C was used for the ROP of *rac*-LA (131 mg, 0.909 mmol) using the PF$_{5k}$-(OH)$_3$ macroinitiator ($M_{n,NMR}$ = 5500 g mol^{-1}; 123 mg, 22.4 μmol) and DBU (1.4 μL, 0.91 μmol) in CH_2Cl_2 (0.913 mL) for 8 min to produce PF$_{5k}$-*b*-(PLA)$_3$ (246 mg) as a light yellow powder. Yield: 96.9%. $M_{n,SEC}$ = 14000 g mol^{-1}; $M_{n,NMR}$ = 10500 g mol^{-1}; $Đ$ = 1.19. ^{1}H NMR ($CDCl_3$, 400MHz) ppm: 7.85-7.20 (br, Ar-*H*)), 5.19 (m, -C(=O)C*H*CH_3O), 4.42-4.26 (m,

-C*H*$_2$(CH$_2$)$_5$O-, -C(=O)C*H*CH$_3$OH), 4.16 (m, -C(C*H*$_2$O-PLA)$_3$), 3.34 (m, -C*H*$_2$OC*H*$_2$-), 2.80 (s, -OC(=O)CH$_2$CH$_2$C*H*$_2$-), 2.12 (br, -C*H*$_2$(CH$_2$)$_4$CH$_3$), 1.89 (m, -OC(=O)CH$_2$C*H*$_2$CH$_2$-), 1.58 (m, -C(=O)C*H*$_3$CHO-), 1.40-0.60 (m, -CH$_2$(C*H*$_2$)$_4$C*H*$_3$).

Bulk sample preparation. The PF-*b*-(PLA)$_x$ block copolymer (5 mg) was dissolved in chloroform (1 mL) and subsequently placed in a 1 mL Teflon beaker to evaporate the solvent at room temperature. The bulk sample was then initially annealed at 180 °C for 3 h, then another 72 h at 140 °C.

Transmission electron microscopy (TEM) measurement. For the transmission electron microscopy (TEM) measurement, the thermal-annealed bulk sample was first embedded in epoxy resin, cured at 60 °C for 6 h, then cut into thin slices with the approximate thickness of 80 nm by a microtome machine. The cut slice was then stained with RuO_4 vapor to enhance the contrast of the PF block. The TEM images were obtained using a JEOL JEM-1230 transmission electron microscope at the accelerating voltage of 100 kV.

Small-angle X-ray scattering (SAXS) measurement. The small angle X-ray scattering (SAXS) measurement was performed on beamline BL 23A1 in the National Synchrotron Radiation Research Center (NSRRC, Hsinchu, Taiwan). A monochromatic beam of λ = 0.887 Å (15 KeV) was used. SAXS profiles were collected by a Pilatus 1 M detector with an area of 169 mm × 179 mm (981 pixels × 1043 pixels). The 1-D scattering intensity profiles were obtained by circularly averaging the 2-D pattern and reported as the plots of the I versus q, where I is the scattering

intensity and q is the scattering vector defined as following equation:

$$q = \frac{4\pi}{\lambda} \sin\left(\frac{\theta}{2}\right)$$

where λ is the wavelength of the incident X-rays and θ is the scattering angle.

Results and Discussion

Synthesis of polyfluorene-based macroinitiators. Our initial effort was directed toward the establishment of a precise synthetic method for the benzylalcohol end-functionalized poly[2,7-(9,9-dihexylfluorene)] (PF-BnOH) with the narrow dispersity (*Đ*) and high level of end-group fidelity, which is very important for the access to well-defined BCPs. Recently, Hu et al. reported the sophisticated synthesis of PFs through the chain growth Suzuki-Miyaura coupling polymerization with the intrinsic initiator that consisted of *p*-substituted iodobenzene derivatives, $Pd_2(dba)_3$, and *t*-Bu_3P, in which the *p*-substituted phenyl group is incorporated at the α-chain end.[57,58] However, the use of 4-(tetrahydropyran-2'-yloxymethyl)-iodobenzene (**1**) as the initiator using Hu's procedure has never been reported. According to the reported polymerization condition, we first attempted the polymerization of 2-(7-bromo-9,9-dihexyl-9*H*-fluorene-2-yl)4,4,5,5-tetramethyl-1,2,3-dioxaborolane (**2**) using the **1**/$Pd_2(dba)_3$/*t*-Bu_3P initiating system at the $[\mathbf{2}]_0/[\mathbf{1}]_0/[K_3PO_4]_0$ ratio of 5/1/50 at 0 °C in THF/H_2O ($[\mathbf{2}]_0$ = 17 mmol L^{-1}). Unfortunately, the obtained PF ($M_{n,SEC}$ = 11200 g mol^{-1}) was found to have a broad distribution with the *Đ* value of 1.75 (run 1, Table 1). Therefore, we thoroughly optimized the polymerization conditions to produce a narrowly-dispersed PF. Lowering the monomer concentration ($[\mathbf{2}]_0$ = 8.0 mmol L^{-1}) did not affect the *Đ* value (run 2), whereas the increase in the concentration of K_3PO_4 ($[\mathbf{2}]_0/[\mathbf{1}]_0/[K_3PO_4]_0$ = 5/1/150) produced a PF with the relatively narrow *Đ* value of 1.45 (run 3). Furthermore, the addition of 18-crown-6 ($[\mathbf{2}]_0/[\mathbf{1}]_0/[K_3PO_4]_0/[\text{18-crown-6}]_0$ =

5/1/150/50) led to a significant improvement in the *Đ* value of the resulting PF ($M_{n,SEC}$ = 6300 g mol^{-1}, *Đ* = 1.34, run 4). Thus, the chain growth Suzuki-Miyaura coupling polymerization of **2** in the presence of 30 eq. and 10 eq. of K_3PO_4 and 18-crown-6, respectively, was found to be the best condition to produce the narrowly-dispersed PFs. With this optimized condition in hand, the polymerization of **2** was conducted at the [**2**]$_0$/[**1**]$_0$/[K_3PO_4]/[18-crown-6] ratio of 2.5/1/75/25, producing a PF with the $M_{n,SEC}$ and *Đ* values of 3900 g mol^{-1} and 1.26, respectively (run 5).

Table 1. Chain growth Suzuki-Miyaura coupling polymerization of 2-(7-bromo-9,9-dihexyl-9*H*-fluorene-2-yl)4,4,5,5-tetramethyl-1,2,3-dioxaborolane (**2**) using the 4-(tetrahydropyran-2'-yloxymethyl)-iodobenzene (**1**)/$Pd_2(dba)_3$/*t*-Bu_3P initiating system [a]

run	[**2**]$_0$/[**1**]$_0$/[K_3PO_4]/[18-crwon-6]	[**2**]$_0$ (mmol L^{-1})	time (min)	$M_{n,SEC}$ [b] (g mol^{-1})	*Đ* [b]	yield (%)
1 [c]	5/1/50/0	17	30	11200	1.75	37.4
2	5/1/50/0	8.0	90	13400	1.73	40.9
3	5/1/150/0	8.0	90	7900	1.45	56.3
4	5/1/150/50	8.0	90	7000 [d]	1.34	91.4
5	2.5/1/75/25	8.0	45	3900 [e]	1.26	86.9

[a] Polymerization condition: Ar atmosphere; solvent, THF; temp., −10 °C. [b] Determined by SEC in THF using polystyrene standard. [c] Temp., 0 °C. [d] $M_{n,NMR}$ = 4800 g mol^{-1}. [e] $M_{n,NMR}$ = 2800 g mol^{-1}.

The chemical structures of the obtained PFs were identified by ^{1}H NMR analyses. In the ^{1}H NMR spectrum of the PF obtained from run 4 (Figure 1a), the major signals due to the fluorene backbone (7.93 – 7.57 ppm: proton *A*) and hexyl side chain (2.12: proton *B*, 1.36 – 0.66 ppm: proton *C* and *D*) were observed, which are consistent with the reported ^{1}H NMR data.[57,58] In addition, a minor signal due to the benzyl proton located at the *α*-chain end (proton *a*) was observed at 4.79 ppm,

suggesting the successful incorporation of the initiator residue. The end group analysis based on the ^{1}H NMR spectra provided the absolute number average molecular weight ($M_{n,NMR}$) of the resultant PFs. The $M_{n,NMR}$ values of the PFs obtained from runs 4 and 5 were calculated to be 4800 and 2800 g mol^{-1}, respectively. To further confirm the end group fidelity, matrix-assisted laser desorption/ionization time-of-flight mass (MALDI-TOF MS) spectrometry was employed for the obtained PF (run 4). The MALDI-TOF MS spectrum (Figure 2a) showed one series of peaks with a regular interval of 332 Da corresponding to the 9,9-dihexylfluorene repeating units. The observed peaks were assigned to the expected chemical structure of PF-BnOH having a benzyl alcohol moiety at the α-chain end and a proton at the ω-chain end because one of the peaks at 4764.48 Da matched well with the calculated mass for the 14-mer of PF-BnOH ($[M + H]^+$ = 4763.58 Da). Although minor unassignable peaks were observed in the range of 1000 – 4000 Da, the end group fidelity was estimated to be >95% by the MALDI-TOF MS analysis. Thus, the well-defined PFs possessing a benzyl alcohol moiety, i.e., PF-BnOH, with a sufficient end group fidelity were produced.

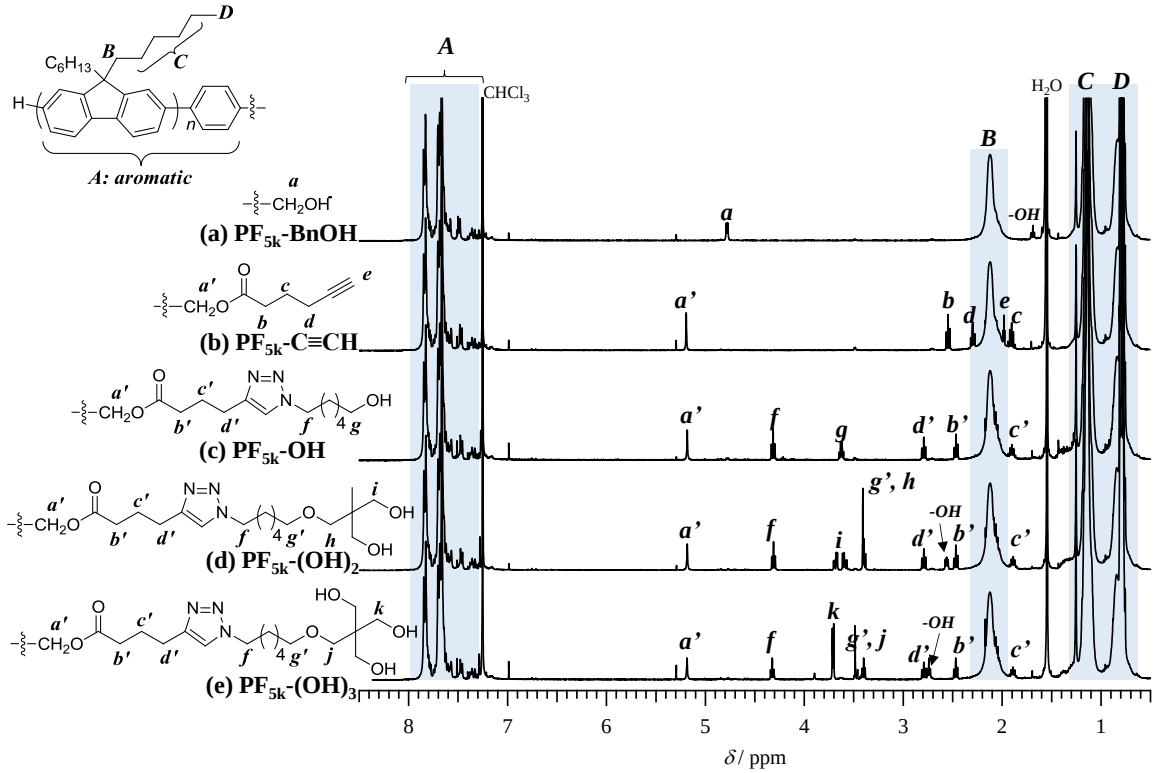

Figure 1. ^{1}H NMR spectra of (a) PF_{5k}-BnOH ($M_{n,NMR}$ = 4800 g mol^{-1}, $Đ$ = 1.34), (b) PF_{5k}-C≡CH ($M_{n,NMR}$ = 4900 g mol^{-1}, $Đ$ = 1.31), (c) PF_{5k}-OH ($M_{n,NMR}$ = 5000 g mol^{-1}, $Đ$ = 1.29), (d) PF_{5k}-$(OH)_2$ ($M_{n,NMR}$ = 5500 g mol^{-1}, $Đ$ = 1.22), and (e) PF_{5k}-$(OH)_3$ ($M_{n,NMR}$ = 5500 g mol^{-1}, $Đ$ = 1.21) in $CDCl_3$ (400 MHz).

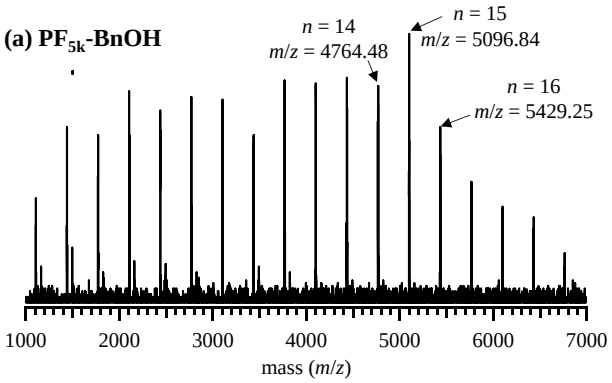

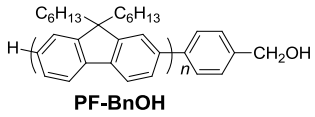

PF-BnOH

	***n* = 14**	***n* = 15**	***n* = 16**
Clcd.	**4763.58**	**5096.83**	**5429.09**
Found	**4764.48**	**5096.84**	**5429.25**

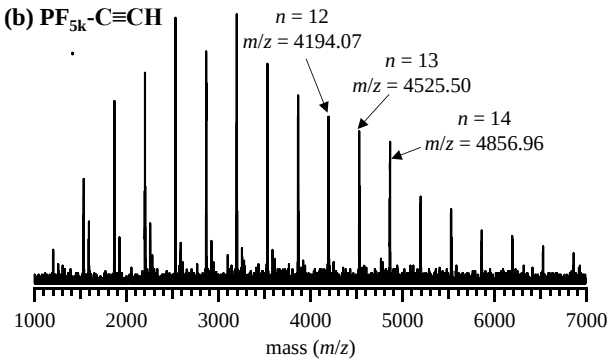

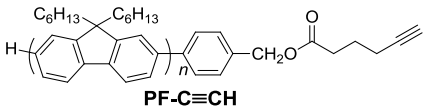

PF-C≡CH

	***n* = 12**	***n* = 13**	***n* = 14**
Clcd.	**4193.12**	**4525.37**	**4857.62**
Found	**4194.07**	**4525.50**	**4856.96**

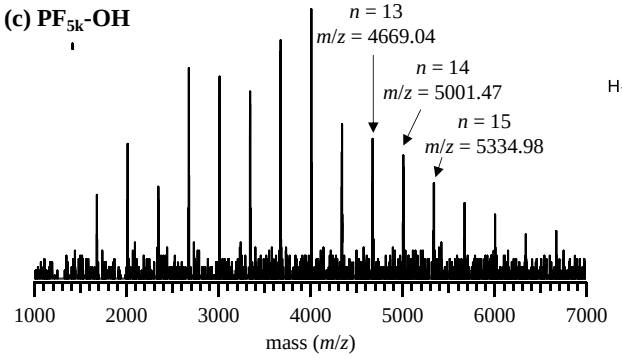

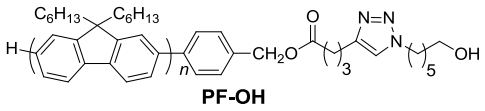

PF-OH

	***n* = 13**	***n* = 14**	***n* = 15**
Clcd.	**4668.48**	**5000.73**	**533.98**
Found	**4669.04**	**5001.47**	**5334.98**

Figure 2. MALDI-TOF MS spectral analysis of (a) PF_{5k}-BnOH ($M_{n,NMR}$ = 4800 g mol^{-1}, $Đ$ = 1.34), (b) PF_{5k}-C≡CH ($M_{n,NMR}$ = 4900 g mol^{-1}, $Đ$ = 1.31), and (c) PF_{5k}-OH ($M_{n,NMR}$ = 5000 g mol^{-1}, $Đ$ = 1.29).

With the well-defined PFs in hand, we next prepared the PF macroinitiators possessing one, two, and three hydroxyl groups at the α-chain end (PF-OH, PF-$(OH)_2$, and PF-$(OH)_3$, respectively). As shown in Scheme 1, PF-BnOH was first converted to an ethynyl end-functionalized PF (PF-C≡CH) by the esterification with 5-hexynoic acid, then further modified by the click reaction with **3**, **4**, and **5** to afford PF-OH, PF-$(OH)_2$, and PF-$(OH)_3$, respectively. The esterification of

PF-BnOH with 5-hexynoic acid was carried out in CH_2Cl_2 at room temperature for 24 h with the aid of EDC and DMAP, producing the PF-C≡CHs in good yields (77.2% for $PF_{2.5k}$-C≡CH and 98.4% for PF_{5k}-C≡CH). The complete conversion from PF-BnOH to PF-C≡CH was verified by the replacement of the benzyl proton adjacent to the hydroxyl group of PF-BnOH observed at 4.79 ppm by the new signal at 5.20 ppm due to the benzyl proton adjacent to the hexynoate residue (proton *a'*; Figure 1b). The signal due to the ethynyl proton (proton *e*) was also visible at 1.98 ppm in the ^{1}H NMR spectrum. The MALDI-TOF MS analysis also supported this conclusion (Figure 2b). The MALDI-TOF MS spectrum of PF_{5k}-C≡CH obtained from PF_{5k}-BnOH revealed the absence of the peak due to the remaining starting material. In addition, one of the observed peaks at 4525.50 Da matched the calculated mass for the 13-mer of PF-C≡CH ($[M + H]^+$ = 4525.37), ensuring the quantitative end group conversion. The obtained PF-C≡CHs were then subjected to the click reaction with **3**, **4**, and **5** in the presence of CuCl/PMDETA in THF at room temperature for 48 h to produce PF-OH, PF-$(OH)_2$, and PF-$(OH)_3$, respectively, in sufficient yields (48.0 – 95.0%). The ^{1}H NMR spectra of the obtained PF-OH, PF-$(OH)_2$, and PF-$(OH)_3$ revealed the absence of the signal due to the ethynyl proton observed at 1.98 ppm, strongly suggesting that there is no unreacted ethynyl group in the products. In addition, the signals due to the methylene protons adjacent to the hydroxyl group were newly observed in each product (proton *g* at 3.63 ppm for PF-OH; proton *i* at 3.72 – 3.52 ppm for PF-$(OH)_2$; proton *k* at 3.71 ppm for PF-$(OH)_3$). The other ^{1}H NMR signals were reasonably assigned to the expected structure of PF-OH, PF-$(OH)_2$, and PF-$(OH)_3$, as shown in

Figure 1c-e. To further confirm the chemical structures, MALDI-TOF MS measurements were performed on the obtained PF_{5k}-OH, PF_{5k}-$(OH)_2$, and PF_{5k}-$(OH)_3$. Figure 2c depicts the MALDI-TOF MS spectrum of PF_{5k}-OH as a representative example. Only one series of peaks corresponding to the expected structure of PF-OH was observed in the spectrum, indicative of the sufficient purity of the obtained PF_{5k}-OH macroinitiator. For example, the peak at 5334.98 Da corresponded to the calculated mass for the 15-mer of PF-OH ($[M + H]^+$ = 5334.98). Similar results were also obtained for all the other macroinitiators (MALDI-TOF MS spectra of PF_{5k}-$(OH)_2$ and PF_{5k}-$(OH)_3$ are shown in Figures S1a and b, respectively). Thus, a series of PF-based macroinitiators possessing multiple hydroxyl groups was found to be accessible by the chain-growth Suzuki-Miyaura coupling polymerization followed by end group modifications.

Table 2. Molecular characteristics of PF macroinitiators possessing one, two, and three hydroxyl groups at the α-chain end (PF-OH, PF-$(OH)_2$, and PF-$(OH)_3$, respectively)

	$M_{n,NMR}$ [a] (g mol^{-1})	$M_{n,SEC}$ [b] (g mol^{-1})	$Đ$ [b]	yield (%)
$PF_{2.5k}$-OH [c]	2700	5200	1.21	84.5
$PF_{2.5k}$-$(OH)_2$ [c]	2800	5600	1.24	65.0
$PF_{2.5k}$-$(OH)_3$ [c]	2800	5100	1.26	61.5
PF_{5k}-OH [d]	5000	7800	1.29	95.0
PF_{5k}-$(OH)_2$ [d]	5500	9300	1.22	79.0
PF_{5k}-$(OH)_3$ [d]	5500	9400	1.21	48.0

[a] Determined by ^{1}H NMR in $CDCl_3$. [b] Determined by SEC in THF using polystyrene calibration. [c] Prepared from $PF_{2.5k}$-C≡CH ($M_{n,NMR}$ = 2600 g mol^{-1}; $M_{n,SEC}$ = 4600 g mol^{-1}; $Đ$ = 1.23). [d] Prepared from PF_{5k}-C≡CH ($M_{n,NMR}$ = 4900 g mol^{-1}; $M_{n,SEC}$ = 7300 g mol^{-1}; $Đ$ = 1.31).

Synthesis and characterization of diblock and miktoarm star copolymers consisting of

polyfluorene and polylactide. The AB type diblock copolymers as well as the AB_2 and AB_3 type miktoarm star copolymers consisting of PF (as A block) and PLA (as B block) were prepared by the ROP of *rac*-LA using the PF-OH, PF-$(OH)_2$, and PF-$(OH)_3$ macroinitiators. We previously found that the star-shaped PLAs having the requisite arm numbers could be obtained by the DBU-catalyzed ROP coupled with multiple hydroxyl-functionalized initiators.[26,61] Therefore, we employed DBU as the catalyst for the BCP synthesis. In order to obtain a series of BCPs with two different weight fractions of the PF block (f_{PF}), the [*rac*-LA]$_0$/[macroinitiator]$_0$ ratios of ca. 60/1 and ca. 40/1 were used for the $PF_{2.5k}$-$(OH)_x$ and PF_{5k}-$(OH)_x$ (x = 1, 2, and 3) series macroinitiators, respectively. The ROPs were conducted in the presence of 1 mol% DBU in CH_2Cl_2 at room temperature, and the BCPs were obtained as a light yellow powder in 48.8 – 97.3% yields after reprecipitation. Table 3 summarizes the results for the BCP synthesis. Figures 3 and S2 show the SEC traces of the obtained BCPs together with the corresponding macromonomers. The elution peak of the macromonomer shifted to the higher molecular weight region after the DBU-catalyzed ROP of *rac*-LA, indicating that the ROP was initiated from the corresponding macroinitiators. The ^{1}H NMR spectra of the products (Figure 4a – c) showed the major signals due to PLA backbone (protons α and β) as well as PF backbone (protons *A*, *B*, *C*, and *D*) along with minor signals due to the junction between the PF and PLA block. In addition, the signals assignable to the methine proton adjacent to the ω-end hydroxyl group of the PLA block (proton γ) were observed at 4.35 ppm, from which the requisite PLA arm number was verified. These ^{1}H NMR and SEC analyses

confirmed that the desired BCPs consisting of the PF and PLA blocks were successfully obtained. The f_{PF} of the obtained BCPs were calculated to be 0.52 – 0.56 for the PF_{5k}-*b*-$(PLA)_x$ series and 0.22 – 0.23 for the $PF_{2.5k}$-*b*-$(PLA)_x$ series (x = 1, 2, and 3 for AB, AB_2, and AB_3 type BCPs, respectively).

Table 3. Molecular characteristics of PF-*b*-PLAs, PF-*b*-$(PLA)_2$s, and PF-*b*-$(PLA)_3$s

sample	$M_{n,NMR}$ [a] (g mol^{-1})	$M_{n,SEC}$ [b] (g mol^{-1})	$Đ$ [b]	f_{PF} [c]	yield (%)
$PF_{2.5k}$-*b*-PLA	12300	13000	1.20	0.22	97.3
$PF_{2.5k}$-*b*-$(PLA)_2$	12000	10800	1.29	0.23	48.8
$PF_{2.5k}$-*b*-$(PLA)_3$	12000	10300	1.26	0.23	52.9
PF_{5k}-*b*-PLA	9200	12000	1.15	0.54	76.5
PF_{5k}-*b*-$(PLA)_2$	9800	12200	1.17	0.56	84.7
PF_{5k}-*b*-$(PLA)_3$	10500	14000	1.19	0.52	96.9

[a] Determined by ^{1}H NMR in $CDCl_3$. [b] Determined by SEC in THF using polystyrene calibration. [c] Weight fraction of the PF block.

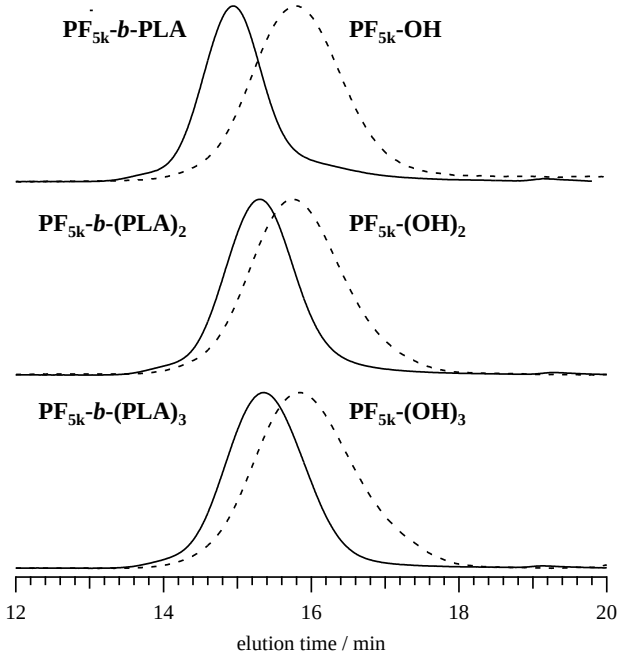

Figure 3. SEC traces of PF_{5k}-*b*-$(PLA)_x$s (x = 1, 2, and 3; solid curves) and the corresponding macroinitiators, PF_{5k}-$(OH)_x$s (x = 1, 2, and 3; broken curves).

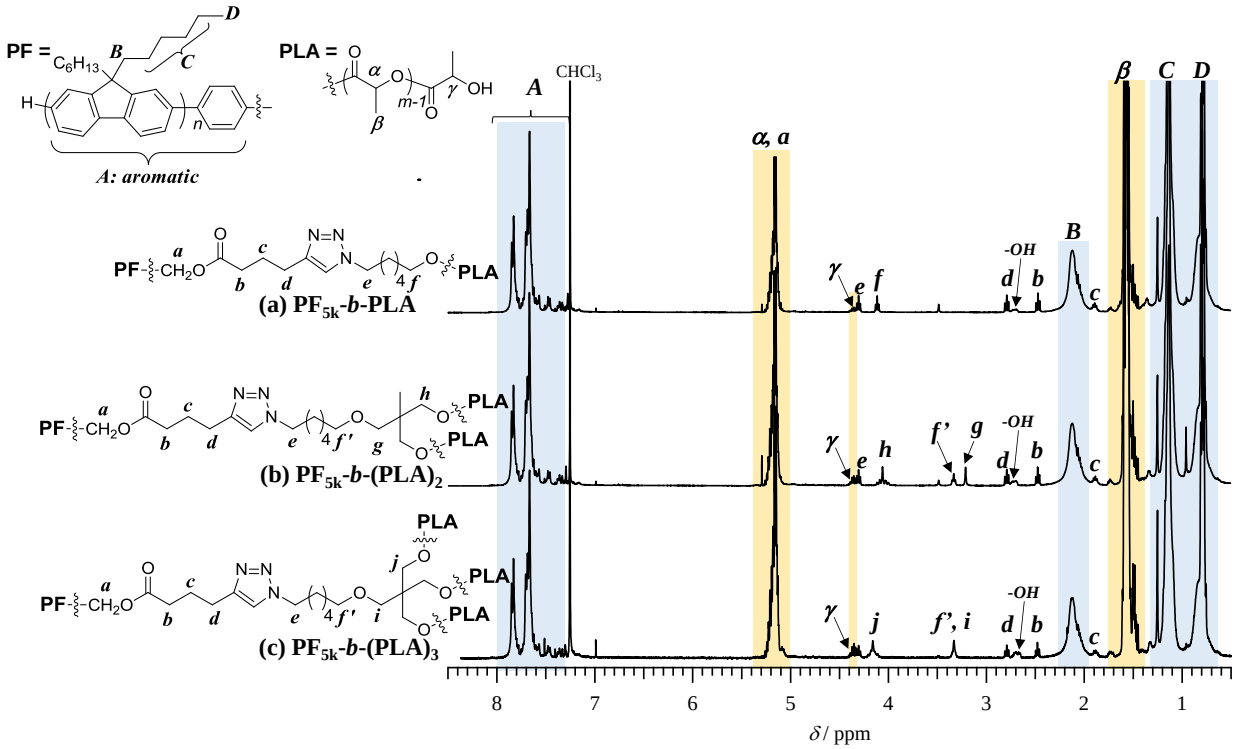

Figure 4. ^{1}H NMR spectra of (a) PF_{5k}-*b*-PLA ($M_{n,NMR}$ = 9400 g mol^{-1}; $M_{n,SEC}$ = 12000 g mol^{-1}; $Đ$ = 1.15), (b) PF_{5k}-*b*-$(PLA)_2$ ($M_{n,NMR}$ = 9800 g mol^{-1}; $M_{n,SEC}$ = 12200 g mol^{-1}; $Đ$ = 1.17), and (c) PF_{5k}-*b*-$(PLA)_3$ ($M_{n,NMR}$ = 10500 g mol^{-1}; $M_{n,SEC}$ = 14000 g mol^{-1}; $Đ$ = 1.19) in $CDCl_3$ (400 MHz).

All the obtained BCPs were soluble in $CHCl_3$, THF, toluene, acetone, and DMF, but insoluble in *n*-hexane and MeOH. Noteworthy is that the PF homopolymer was insoluble in acetone and DMF, suggesting that the PLA block endowed the BCPs with an increased solubility in such polar solvents. The thermal properties of the BCPs were investigated in a dry nitrogen atmosphere by TGA and DSC measurements. The TGA profile revealed that the thermal degradation of the PF_{5k}-*b*-PLA occurred in two steps, in which the first (ca. 270 °C) and second steps (ca. 410 °C) of the degradation stages are attributed to the PLA and PF blocks, respectively (Figure S3). A similar two-step degradation behavior was observed for the TGA profiles of the other BCPs,

and the thermal decomposition temperatures for a 5% weight loss ($T_{d,5\%}$) were in the range of 262 – 301 °C. In the second heating DSC traces, all the BCPs displayed two independent glass transition temperatures (T_gs) at ca. 40 °C and ca. 60 °C corresponding to the PLA and PF blocks (Figure S4), which is an indication of the microphase separation between these two blocks.

Morphological investigation. The morphological structures of the BCPs in the bulk state were studied using synchrotron small-angle X-ray scattering (SAXS) measurements as well as transmission electron microscope (TEM) observations. We first examined the morphologies of the PF_{5k}-*b*-$(PLA)_x$ series with various branched architectures, i.e., PF_{5k}-*b*-PLA, PF_{5k}-*b*-$(PLA)_2$, and PF_{5k}-*b*-$(PLA)_3$. Note that those BCP samples have comparable molecular weight and composition, as discussed above. We found that the two-step heating at 180 °C for 3 h and subsequent 140 °C for 48 h under high vacuum led to the formation of the nanostructures as discussed below. The thermal treatment at 180 °C was essential in order to remove the thermal history, though the prolonged heating at 180 °C led to less ordered morphology due to the decrease in the Flory-Huggins interaction parameter (χ) value of the BCPs. Figure 5a shows the TEM images of the PF_{5k}-*b*-PLA sample, which were obtained by the staining using RuO_4 vapor for 10 min. The PF segment can be selectively stained, therefore, the dark and bright regions in the TEM image are assignable to the PF and PLA phases, respectively. The TEM image of PF_{5k}-*b*-PLA revealed the presence of a striped morphology with long persistent lengths in a large area. As can be seen in Figure 5b, the SAXS profile of PF_{5k}-*b*-PLA displayed a first order scattering peak (q^*) at 0.0324 $Å^{-1}$, suggesting the

formation of certain thermodynamically stable phases. The domain-spacing (d) was calculated to be 19.3 nm based on Bragg's equation ($d = 2\pi/q^*$). Unfortunately, the exact phase structure was not identified by the SAXS profile due to the lack of a distinct higher order scattering peak. The SAXS profile implies that the higher weight fraction of PF in the BCP result in the suppression of long-range lateral ordering of the nanostructure mainly due to the strong π-π stacking interaction between the PF chains. We tentatively attributed the observed morphologies to the cylindrical structures with the PF continuous phase. Similarly, PF_{5k}-*b*-$(PLA)_2$ and PF_{5k}-*b*-$(PLA)_3$ were found to show striped morphologies corresponding to the cylindrical structures, as can be seen in their TEM images (Figures 5c and e). The SAXS profiles of PF_{5k}-*b*-$(PLA)_2$ and PF_{5k}-*b*-$(PLA)_3$ showed a first order peak at 0.0296 $Å^{-1}$ and 0.0260 $Å^{-1}$, respectively, from which the domain-spacing values for the PF_{5k}-*b*-$(PLA)_2$ and PF_{5k}-*b*-$(PLA)_3$ samples were calculated to be 21.2 nm and 24.2 nm, respectively (Figures 5d and f). The lack of a distinct higher ordered scattering peak in their SAXS profiles suggests that PF_{5k}-*b*-$(PLA)_2$ and PF_{5k}-*b*-$(PLA)_3$ also formed poorly ordered cylindrical structures as a consequence of the strong interaction between the PF chains. Interestingly, the domain-spacing values among the PF_{5k}-*b*-$(PLA)_x$ series were found to increase with the increasing arm number of the PLA block; 19.3 nm for PF_{5k}-*b*-PLA, 21.2 nm for PF_{5k}-*b*-$(PLA)_2$, and 24.2 nm for PF_{5k}-*b*-$(PLA)_3$. This tendency can also be confirmed by the TEM images. Figure S5a depicts the contrast profiles for the striped regions in the TEM images, where the pitches between the domains were slightly increased with the increasing PLA branching. In case of the PF_{5k}-*b*-$(PLA)_x$ series, the

strong π-π interaction should dominated the microphase separation behavior. The TEM images shown in Figures 5c and 5e clearly revealed that the random orientation of the cylindrical structures became more pronounced with the increasing arm number of the PLA. This observation implied that the interface between the PF and PLA blocks became unstable with the increasing arm number of the PLA block due to the steric hindrance of the branch, which resulted in enhancing the PF aggregation and increasing the domain-spacing value accordingly. Nevertheless, these results demonstrate that the nanostructure formation in the rod-coil BCP can be turned by introducing branching in the coil block.

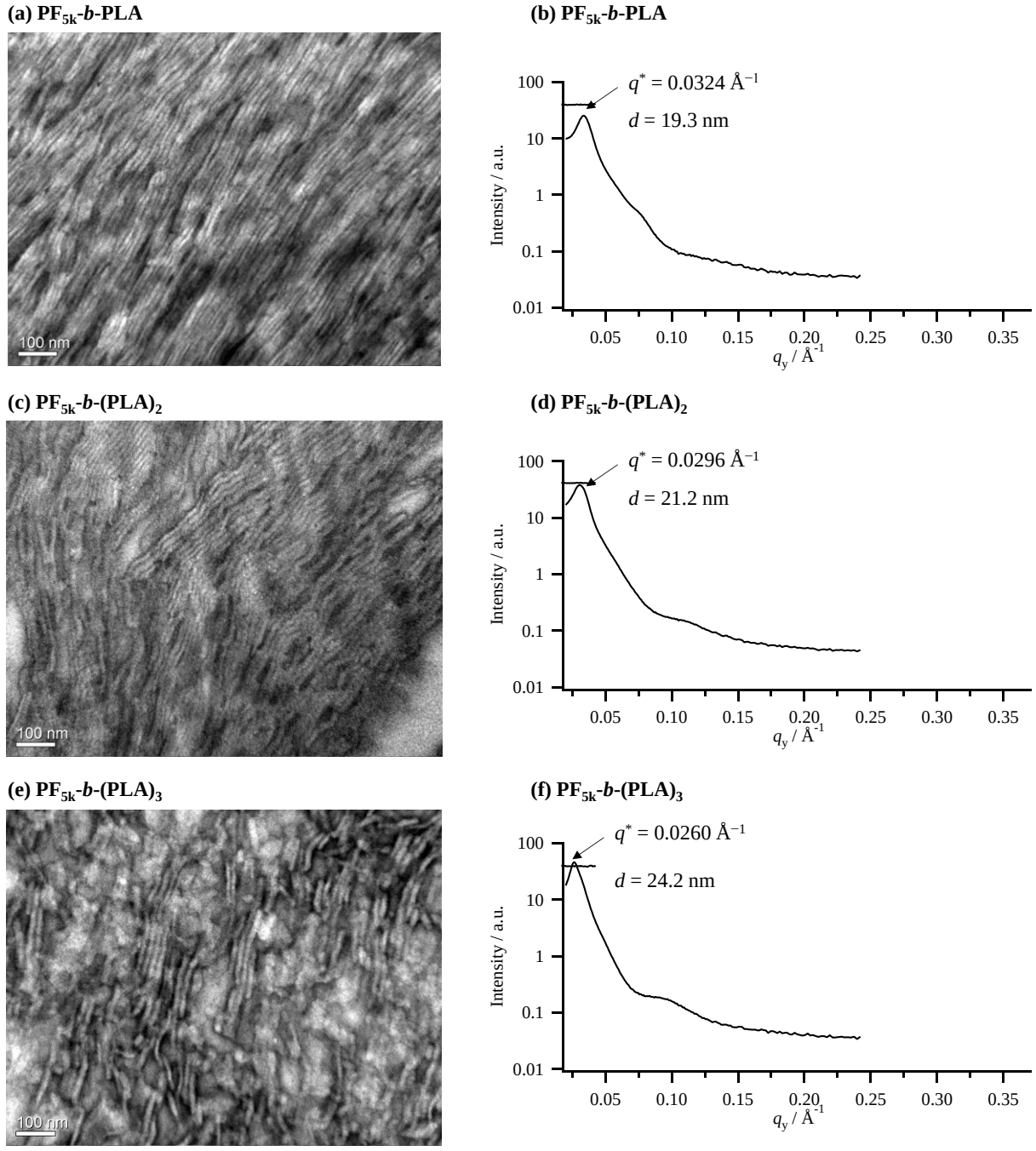

Figure 5. TEM images and SAXS profiles for the thermally-annealed bulk samples of PF_{5k}-*b*-PLA (a and b), PF_{5k}-*b*-$(PLA)_2$ (c and d), and PF_{5k}-*b*-$(PLA)_3$ (e and f).

We next investigated the morphological characteristics of the $PF_{2.5k}$-*b*-$(PLA)_x$ series that have the lower f_{PF} values of 0.22 – 0.23. For $PF_{2.5k}$-*b*-PLA, the strip morphologies corresponding to the cylindrical structures were visible in the TEM image (Figure 6a). To gain further information

about the morphology, a SAXS measurement was carried out on the bulk sample (Figure 6b). In contrast to the case of PF_{5k}-*b*-PLA, the bulk samples of $PF_{2.5k}$-*b*-PLA exhibited a sharp first order scattering peak (q^*) at 0.0238 $Å^{-1}$ with higher order scattering peaks at $\sqrt{3}q^*$ and$\sqrt{7}q^*$, demonstrating the formation of a hexagonally close-packed cylinder (Hex) phase. Given that the major component of the BCP is the PLA block, the cylindrical domain made by PF should be embedded in the PLA matrix. Therefore, the higher coil weight fraction enabled the formation of well-ordered microphase-separated structures, as is known for the conventional coil-coil BCP system. A similar conclusion was found in the polythiophene-based rod-coil BCP, i.e., poly(3-hexyl thiophene)-*b*-poly(2-vinylpyridine).[62]

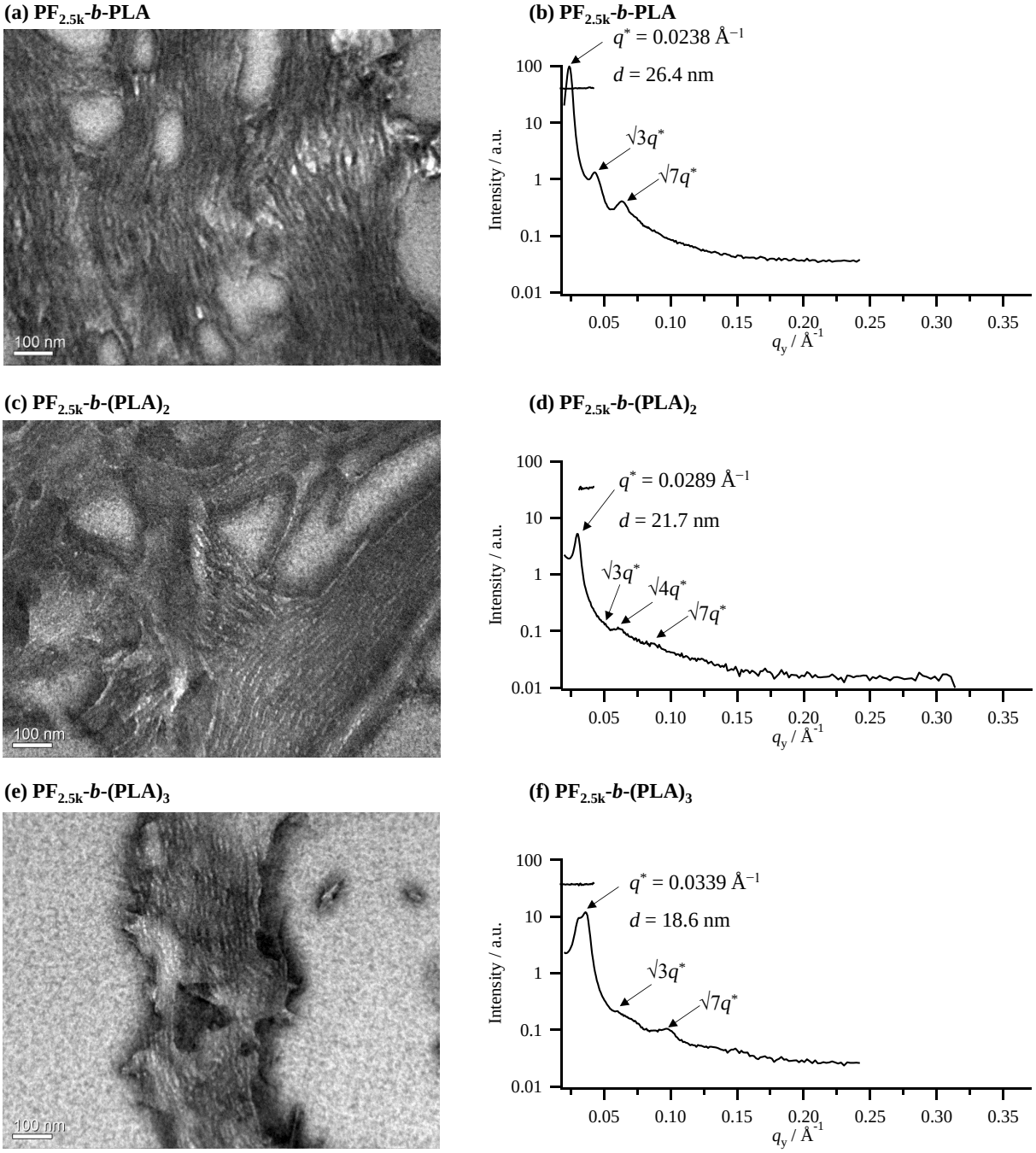

Figure 6. TEM images and SAXS profiles for the thermally-annealed bulk samples of $PF_{2.5k}$-*b*-PLA (a and b), $PF_{2.5k}$-*b*-$(PLA)_2$ (c and d), and $PF_{2.5k}$-*b*-$(PLA)_3$ (e and f).

To further clarify the effect of the branched PLA architecture, TEM and SAXS experiments were performed on the bulk $PF_{2.5k}$-*b*-$(PLA)_2$ and $PF_{2.5k}$-*b*-$(PLA)_3$ samples (Figures 6c-f). The striped morphologies were confirmed from the TEM images of both the $PF_{2.5k}$-*b*-$(PLA)_2$ and

$PF_{2.5k}$-*b*-$(PLA)_3$ samples, which resembled those of the Hex morphology observed in the $PF_{2.5k}$-*b*-PLA sample. Indeed, the SAXS profiles of both $PF_{2.5k}$-*b*-$(PLA)_2$ and $PF_{2.5k}$-*b*-$(PLA)_3$ showed a distinct primary scattering peak with higher order scattering peaks corresponding to the Hex phase. Thus, the branched architecture of the PLA block had a slight effect on the self-assembled morphologies at this rod/coil volume ratio. An interesting feature of the present BCP system occurred by comparing it with Milner's theory[63] that describes the phase behavior of miktoarm star copolymers. Milner's theory roughly predicts that the AB_x type BCP ($x > 2$) with a higher B volume fraction would exhibit a Hex phase and eventually a body-centered cubic (BCC) sphere phase with the increasing branching. On the other hand, for the present $PF_{2.5k}$-*b*-$(PLA)_x$ series with the higher PLA volume fraction, Hex phases were observed irrespective of the arm number of the PLA block. These arguments led to the conclusion that the large deviation between the observed phase behavior and Milner's theory is due to the rod-like nature of the PF block in which the rigidity of the PF chain makes the BCPs difficult to form a curved interface. Nevertheless, the higher coil weight fraction in the PF-based miktoarm star copolymers preferentially leads to an ordered microphase-separated structure, in which the PF chains are packed in the cylindrical domain. This is of key importance in controlling the opto-electronic properties of PF-based devices. In addition, we found that the domain-spacing values of the $PF_{2.5k}$-*b*-$(PLA)_x$ series decreased with the increasing PLA arm number; $PF_{2.5k}$-*b*-PLA for 26.4 nm, 21.7 nm for $PF_{2.5k}$-*b*-$(PLA)_2$, and 18.6 nm for $PF_{2.5k}$-*b*-$(PLA)_3$. The TEM analysis also supported this tendency

(Figure S5b). A plausible explanation for this interesting feature is that branching of the PLA block into shorter arms leads to a decrease in the apparent radius of gyration of the PLA segment, resulting in a closely-packed morphology. A similar tendency was observed for the AB_2 and AB_3 type miktoarm star copolymers consisting of maltoheptaose (as A block) and poly(ε-caprolactone) (as B block), in which the domain-spacing of the resultant body-centered cubic sphere was minimized by the increasing arm number of the B block.[60] Such a controllability of the domain-spacing in the PF-based BCPs should be of interest for the fine turning of the PF-based sensor, OFET, OLED, and memory device performances.[64]

Conclusion

We succeeded in the synthesis of AB_2 and AB_3 type rod-coil miktoarm star copolymers consisting of the PF (A block) and PCL (B block), together with the corresponding linear AB diblock counterparts. The PF-based macroinitiators possessing one, two, and three hydroxyl groups at the α-chain end were obtained by the chain growth Suzuki-Miyaura coupling polymerization. The desired linear diblock and miktoarm star copolymers with the relatively narrow $Đ$ value of less than 1.3 were obtained by the DBU-catalyzed ROP with the corresponding macroinitiators. The bulk samples of all the obtained BCPs were found to self-assemble into nanostructures with the periodicity of 18.6 – 26.4 nm via thermal annealing. The series of BCPs with the f_{PF} value of 0.52 – 0.56, i.e., PF_{5k}-*b*-PLA, PF_{5k}-*b*-$(PLA)_2$, and PF_{5k}-*b*-$(PLA)_3$, showed poorly ordered cylindrical

structures, which can be explained by the higher PF content that lead to the random aggregation of the rod segments through the strong π-π stacking interaction. On the other hand, the series of BCPs with the f_{PF} value of 0.22 – 0.23, i.e., $PF_{2.5k}$-*b*-PLA, $PF_{2.5k}$-*b*-$(PLA)_2$, and $PF_{2.5k}$-*b*-$(PLA)_3$, formed hexagonally-closed packed cylinder morphologies, as can be seen in the SAXS profiles. Thus, the higher coil content is important for the self-assembly into ordered microphase-separated structures. More importantly, we found that the domain-spacing values for the Hex phases of $PF_{2.5k}$-*b*-PLA, $PF_{2.5k}$-*b*-$(PLA)_2$, and $PF_{2.5k}$-*b*-$(PLA)_3$ decreased with the increasing arm number of the PLA block. Since the opto-electronic properties of the main chain-conjugated polymers were found to correlate with their morphology in the solid state, the controllability of the domain-spacing for the rod-coil BCPs should be of high interest as a new factor for the devise design strategy. We are currently investigating the correlation between the memory device performance and nanostructures of the PF-*b*-$(PLA)_x$ BCP samples in order to provide better guidance to produce a variety of digital memory properties.

Acknowledgements

This work was financially supported by the MEXT Grant-in-Aid for Scientific Research on Innovative Areas “Advanced Molecular Transformation by Organocatalysts” and MEXT Grant-in-Aid for Scientific Research (B) (25288093).

References

1. N. Hadjichristidis, M. Pitsikalis, S. Pispas, H. Iatrou, *Chem. Rev.*, 2001, **101**, 3747.
2. N. Hadjichristidis, H. Iatrou, M. Pitsikalis, J. Mays, *Prog. Polym. Sci.*, 2006, **31**, 1068.
3. N. Akeroyd, B. Klumperman, *Eur. Polym. J.*, 2011, **47**, 1207.
4. T. Yamamoto, Y. Tezuka, *Polym. Chem.*, 2011, **2**, 1930.
5. N. Hadjichristidis, A. Hirao, Y. Tezuka, F. Du Prez, Eds.; *Complex Macromolecular Architectures: Synthesis, Characterization, and Self-Assembly*; John Wiley & Sons, Inc.: New York, 2011.
6. N. Hadjichristidis, *J. Polym. Sci. Part A: Polym. Chem.*, 1999, **37**, 857.
7. K. Khanna, S. Varshney, A. Kakkar, *Polym. Chem.*, 2010, **1**, 1171.
8. K. Ishizu, S. Uchida, *Prog. Polym. Sci.*, 1999, **24**, 1439.
9. H. Iatrou, N. Hadjichristidis, *Macromolecules*, 1992, **25**, 4649.
10. H. Iatrou, N. Hadjichristidis, *Macromolecules*, 1993, **26**, 2479.
11. A. Avgeropoulos, Y. Poulos, N. Hadjichristidis, J. Roovers, *Macromolecules*, 1996, **29**, 6076.
12. G. Velis, N. Hadjichristidis, *Macromolecules*, 1999, **32**, 534.
13. A. Hirao, T. Higashihara, *Macromolecules*, 2002, **35**, 7238.
14. T. Higashihara, M. Nagura, K. Inoue, N. Haraguchi, A. Hirao, *Macromolecules*, 2005, **38**, 4577.
15. A. Hirao, T. Higashihara, K. Inoue, *Macromolecules*, 2008, **41**, 3579.
16. S. Ito, R. Goseki, T. Ishizone, S. Senda, A. Hirao, *Macromolecules*, 2013, **46**, 819.

17. T. Higashihara, M. Hayashi, A. Hirao, *Macromolecules*, 2011, **36**, 323.

18. S. Ito, R. Goseki, T. Ishizone, A. Hirao, *Eur. Polym. J.*, 2013, **49**, 2545.

19. D. Proftis, M. Pitsikalis, N. Hadjichristidis, *J. Polym. Sci. Part A: Polym. Chem.*, 2007, **45**, 5164.

20. S. Peleshanko, J. Jeong, V. V. Shevchenko, K. K. Genson, Y. Pikus, M. Ornatska, S. Petrash, V. V. Tsukruk, *Macromolecules*, 2004, **37**, 7497.

21. K. Huang, J. Huang, M. Pan, G. Wang, J. Huang, *J. Polym. Sci. Part A: Polym. Chem.*, 2012, **50**, 2635.

22. F. F. Wolf, N. Friedemann, H. Frey, *Macromolecules*, 2009, **42**, 5622.

23. J. Babin, C. Leroy, S. Lecommandoux, R. Borsali, Y. Gnanou, D. Taton, *Chem. Commun.*, 2005, 1993.

24. J. Babin, D. Taton, M. Brinkmann, S. Lecommandoux, *Biomacromolecules*, 2008, **41**, 1384.

25. M. S. Rahman, M. Changez, J.-W. Yoo, C. H. Lee, S. Samal, J.-S. Lee, *Macromolecules*, 2008, **41**, 7029.

26. T. Satoh, N. Naoki, D. Kawato, D. Suemasa, S. Jung, Y. Y. Kim, M. Ree, T. Kakuchi, *Polym. Chem.*, 2014, **5**, 588.

27. Y. Y. Kim, S. Jung, C. Kim, B. J. Ree, D. Kawato, N. Nishikawa, D. Suemasa, T. Isono, T. Kakuchi, T. Satoh, M. Ree, *Macromolecules*, 2014, **47**, 7510.

28. R. Phinjaroenphan, Y. Y. Kim, S. Jung, T. Isono, Y. Satoh, S. Maensiri, S. Rugmai, T. Kakuchi, T. Satoh, M. Ree, *Sci. Adv. Mater.*, 2014, **6**, 2526.

29. J. Park, H. C. Moon, J. K. Kim, *J. Polym. Sci. Part A: Polym. Chem.*, 2013, **51**, 2225.

30. J. Park, H. C. Moon, C. Choi, J. K. Kim, *Macromolecules*, 2015, **48**, 3523.

31. T. Higashihara, S. Ito, S. Fukuta, T. Koganezawa, M. Ueda, T. Ishizone, A. Hirao, *Macromolecules*, 2014, **48**, 245.

32. D. T. McQuade, A. E. Pullen, T. M. Swager, *Chem. Rev.*, 2000, **100**, 2537.

33. S. W. Thomas III, G. D. Joly, T. M. Swager, *Chem. Rev.*, 2007, **107**, 1339.

34. J. H. Burroughes, D. D. C. Bardley, A. R. Brown, R. N. Marks, K. Mackay, R. H. Friend, P. L. Burns, A. B. Holmes, *Nature*, 1990, **347**, 539.

35. M.-C. Choi, Y. Kim, C.-S. Ha, *Prog. Polym. Sci.*, 2008, **33**, 581.

36. A. C. Grimsdale, K. L. Chan, R. E. Martin, P. G. Jokisz, A. B. Holmes, *Chem. Rev.*, 2009, **109**, 897.

37. B. S. Ong, Y. Wu, Y. Li, P. Liu, H. Pan, *Chem. Eur. J.*, 2008, **14**, 4766.

38. F. Cicoira, C. Santato, *Adv. Funct. Mater.*, 2007, **17**, 3421.

39. K. M. Coakley, M. D. McGehee, *Chem. Mater.*, 2004, **16**, 4533.

40. S. Gunes, H. Neugebauer, N. S. Sariciftci, *Chem. Rev.*, 2007, **107**, 1324.

41. G. Li, R. Zhu, Y. Yang, *Nat. Photonics*, 2012, **6**, 153.

42. Q.-D. Ling, D.-J. Liaw, C. Zhu, D. S.-H. Chan, E.-T. Kang, K.-G. Neoh, *Prog. Polym. Sci.*, 2008, **33**, 917.

43. B. Cho, S. Song, Y. Ji, T.-W. Kim, T. Lee, *Adv. Funct. Mater.*, 2011, **21**, 2806.

44. D. Neher, *Macromol. Rapid Commun.*, 2001, **22**, 1365.

45. U. Scherf, E. J. W. List, *Adv. Mater.*, 2002, **14**, 477.

46. M. Kreyenschmidt, G. Klaerner, T. Fuhrer, J. Ashenhurst, S. Karg, W. D. Chen, V. Y. Lee, J. C. Scott, R. D. Miller, *Macromolecules*, 1998, **31**, 1099.

47. G. Klärner, M. H. Davey, W.-D. Chen, J. C. Scott, R. D. Miller, *Adv. Mater.*, 1998, **10**, 993.

48. D. Marsitzky, M. Klapper, K. Müllen, *Macromolecules*, 1999, **32**, 8685.

49. Y. K. Kwon, H. S. Kim, H. J. Kim, J. H. Oh, H. S. Park, Y. S. Ko, K. B. Kim, M. S. Kim, *Macromolecules*, 2009, **42**, 887.

50. H.-S. Sun, C.-H. Lee, C.-S. Lai, H.-L. Chen, S.-H. Tung, W.-C. Chen, *Soft Matter*, 2011, **7**, 4198.

51. L. Rubatat, X. Kong, S. A. Jenekhe, J. Ruokolainen, M. Hojeij, R. Mezzenga, *Macromolecules*, 2008, **41**, 1846.

52. Y.-C. Chiu, Y. Chen, C.-C. Kuo, S.-H. Tung, T. Kakuchi, W.-C. Chen, *ACS Appl. Mater. Interfaces*, 2012, **4**, 3387.

53. I. Botiz, S. B. Darling, *Macromolecules*, 2009, **42**, 8211.

54. A. Yokoyama, H. Suzuki, Y. Kubota, K. Ohuchi, H. Higashimura, T. Yokozawa, *J. Am. Chem. Soc.*, 2007, **129**, 7236.

55. E. Elmalem, A. Kirity, W. T. S. Huck, *Macromolecules*, 2011, **44**, 9057.

56. U. Mansfeld, M. D. Hager, R. Hoogenboom, C. Ott, A. Winter, U. S. Schubert, *Chem. Commun.*, 2009, 3386.

57. H.-H. Zhang, C.-H. Xing, Q.-S. Hu, K. Hong, *Macromolecules*, 2015, **48**, 967.

58. H.-H. Zhang, C.-H. Xing, Q.-S. Hu, K. Hong, *J. Am. Chem. Soc.*, 2012, **134**, 13156.

59. M. Malkoch, K. Schleicher, E. Drockenmuller, C. J. Hawker, T. P. Russell, P. Wu, V.V. Fokin, *Macromolecules*, 2005, **38**, 3663.

60. T. Isono, I. Otsuka, Y. Kondo, S. Halila, S. Fort, C. Rochas, T. Satoh, R. Borsali, T. Kakuchi, *Macromolecules*, 2013, **46**, 1461.

61. T. Isono, Y. Kondo, I. Otsuka, Y. Nishiyama, R. Borsali, T. Kakuchi, T. Satoh, *Macromolecules*, 2013, **46**, 8509.

62. C.-A. Dai, W.-C. Yen, Y.-H. Lee, C.-C. Ho, W.-F. Su, *J. Am. Chem. Soc.*, 2007, **129**, 11036.

63. S. T. Milner, *Macromolecules*, 1994, **27**, 2333.

64. Y. Tao, B. D. Olsen, V. Ganesan, R. A. Segalman, *Macromolecules*, 2007, **40**, 3320.